# 4 Vibrational Spectroscopy of Intact and Doped Conjugated Polymers and Their Models

*Y. Furukawa and M. Tasumi*

## 4.1 Introduction

Most organic polymers are electrical insulators, a property which distinguishes them from metals. However, the development of a new class of organic polymers with quasimetallic electrical conductivities has been actively pursued during the past 18 years, following the discovery in 1977 of high electrical conductivities for doped polyacetylenes [1, 2]. The novel concept of a conducting organic polymer has aroused the interest of a large number of researchers in various areas such as chemistry, physics, electrical engineering, material science, etc. Detailed discussions in each area can be found in many review articles [3–17]. In particular, a new field of physics has been opened for the purpose of understanding their electrical properties.

A goal of basic research on conducting polymers is to understand the metallic properties of such polymers. Since conducting organic polymers have conjugated $\pi$-electrons in common, chemists intuitively believe that studies on the physical and chemical properties of conjugated systems would lead to an elucidation of the mechanism of charge transport. On the other hand, new concepts, *solitons* [18, 19], *polarons* [20–22], and *bipolarons* [21–23] have been proposed by solid-state physicists as elementary excitations in conjugated polymers, in order to explain the physical properties of these polymers. They are collectively called *self-localized excitations*. These concepts and terminologies are unfamiliar to molecular spectroscopists. Thus, it seems desirable to build a bridge between solid-state physicists and molecular spectroscopists.

The structures and properties of conducting polymers have been studied by various spectroscopic techniques. Among them, vibrational (Raman and infrared) spectroscopy is a powerful tool for elucidating the molecular and electronic structures of conducting polymers as described in previous reviews [13–15]. In spite of numerous spectroscopic studies, discussions on polarons, bipolarons, and solitons were not based upon reliable evidence from vibrational spectroscopy until very recently. Thus, the aims of this review are: (i) to provide a general introduction to the concepts of polarons, bipolarons, and solitons from the standpoint of molecular spectroscopists; (ii) to describe the methodology of Raman studies on these self-localized excitations; (iii) to review the results of studies on poly(*p*-phenylene) and other polymers; and (iv) to discuss the mechanism of charge transport in conducting polymers.

## 4.2 Materials

The conductivity of iodine-doped polyacetylene first reported by Shirakawa et al. [1] in 1977 was 30 S $cm^{-1}$. Since then, the conductivity reported for doped polyacetylene has kept increasing, the highest conductivity obtained so far for an iodine-doped stretched polyacetylene film [17] being $>10^5$ S $cm^{-1}$, a value comparable with that of copper ($6 \times 10^5$ S $cm^{-1}$).

A film of intact polyacetylene usually shows a conductivity lower than $10^{-5}$ S $cm^{-1}$. However, the conductivity increases dramatically when the film is exposed to oxidizing agents (electron acceptors) such as iodine, $AsF_5$, $H_2SO_4$, etc. or reducing agents (electron donors) such as alkali metals. This process is referred to as *doping*, by analogy with the doping of inorganic semiconductors. The polymers that are not doped are referred to as *intact* polymers in this review. The main process of doping is a redox reaction between the polymer chains and acceptors (or donors). Upon doping, an ionic complex consisting of positively (or negatively) charged polymer chains and counter ions such as $I_3^-$, $AsF_6^-$, etc. (or $Na^+$, $K^+$, etc.) is formed. Counter anions or cations are generated by reduction of acceptors or oxidation of donors, respectively. The use of an acceptor causes the p-type doping, and that of a donor the n-type doping. The electrical conductivity can be controlled by the content of a dopant. A sharp increase in conductivity is observed when the dopant content is $<1$ mole% per $C_2H_2$ unit. After this sharp increase, the conductivity becomes gradually higher with further increase in the dopant content. At low doping levels, polyacetylene does not exhibit metallic properties, whereas its conductivity is high. When the dopant content is more than about 13 mole% per $C_2H_2$ unit, polyacetylene shows metallic properties such as a Pauli susceptibility [24, 25], a linear temperature dependence of the thermoelectric power [26], and a high reflectivity in the infrared region [27], though the temperature dependence of conductivity is not like that of a metal. The origin of such properties of heavily doped polyacetylene is not yet fully understood.

Following polyacetylene, a large number of conducting polymers have been reported. The chemical structures of typical conducting polymers are depicted in Figure 4-1. These conducting polymers have conjugated π-electrons in common,

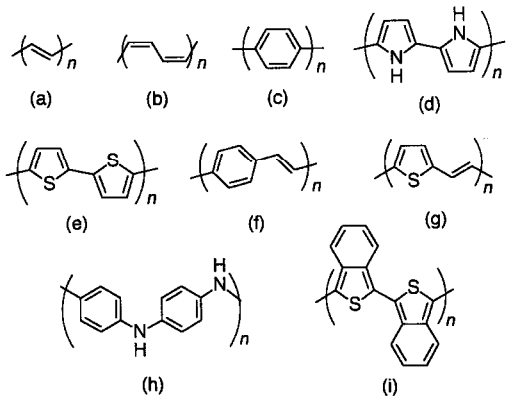


**Figure 4-1.** Chemical structures of conducting polymers. (a) *Trans*-polyacetylene; (b) *cis*-polyacetylene; (c) poly(*p*-phenylene); (d) polypyrrole; (e) polythiophene; (f) poly(*p*-phenylenevinylene); (g) poly(2,5-thienylenevinylene); (h) polyaniline (leucoemeraldine base form); (i) polyisothianaphthene.

and all are either insulators or semiconductors in their intact states, and they become conductors upon doping. Metallic properties are observed for poly(*p*-phenylene) [28], polythiophene [29–33], polypyrrole [31], and polyaniline [34, 35] at heavy doping levels, although reported data depend on samples and preparation methods. The origin of the metallic states of heavily doped polymers is one of the major unresolved problem in the field of conducting polymers.

## 4.3 Geometry of Intact Polymers

The question of whether the C–C bonds in an infinite polyene chain are equal or alternate in length has been discussed by quantum chemists since the 1950s [36, 37]. Various experimental results on oligoenes have shown the existence of alternating single and double bonds. The bond alternation in *trans*-polyacetylene has been confirmed by X-ray [38] and nutation NMR [39] studies. However, it is difficult to determine exact structure parameters for conducting polymers from X-ray diffraction studies, because single crystals of the polymers are unavailable. It is then useful to examine the geometries of the polymers and model oligomers by the molecular orbital (MO) method, especially at *ab initio* Hartree–Fock levels or in higher approximations.

Conducting polymers can be divided into two types, *degenerate* and *nondegenerate*, according to the structure of the ground-states of intact polymers. The total energy curve of a degenerate system in the ground state is shown schematically as a function of a structural deformation coordinate, $R$, in Figure 4-2a, and that for a nondegenerate system in Figure 4-2b. Let us consider an infinite *trans*-polyacetylene chain as a prototype of the degenerate ground-state polymers. There are two degrees of freedom in bond lengths: $r_{C-C}$ and $r_{C=C}$, which correspond, respectively, to the lengths of the alternating single and double CC bonds. The coordinate for structural deformation is simply expressed by the following equation.

$$R = \frac{1}{\sqrt{2}}(r_{C-C} - r_{C=C}) \tag{4-1}$$

This coordinate reflects the degree of bond alternation. This coordinate is used in the effective-conjugation-coordinate model proposed by Zerbi et al. [15] for the purpose

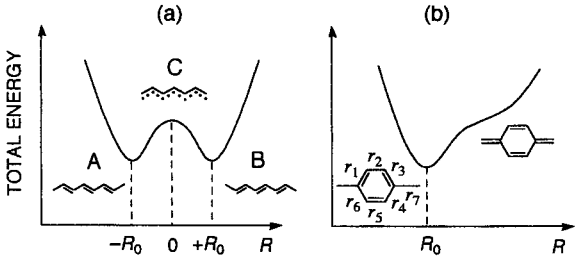


**Figure 4-2.** Total energy as a function of a structural deformation coordinate. (a) *Trans*-polyacetylene (degenerate ground-state system); (b) poly(*p*-phenylene) (nondegenerate ground-state system).

of explaining the Raman spectra of intact polymers and doping-induced infrared bands. (This model will be mentioned again in Section 4.5.) There are two stable structures (A and B in Figure 4-2a) with alternating C–C and C=C bonds, while the structure with equal C–C bond lengths (C in Figure 4-2a) is unstable. These two structures are identical to each other and have the same total energy; in other words, they are degenerate. According to a nutation NMR study [39], the lengths of the C–C and C=C bonds in *trans*-polyacetylene are 1.44 and 1.36 Å, respectively. An ab initio MO calculation at the Hartree–Fock level with the 6-31G basis set for a model compound, $C_{22}H_{24}$, has shown that the C–C and C=C bond lengths of the central unit are 1.450 and 1.338 Å, respectively [40]. Similar results have been obtained from calculations which take into account the effects of electron correlation [41]. From these experimental and theoretical results, $R_0$ (equilibrium value of $R$, see Figure 4-2a) is calculated to be 0.06 and 0.079 Å, respectively.

A nondegenerate polymer has no two identical structures in the ground state. Let us consider poly(*p*-phenylene) as an example of nondegenerate polymers. In order to express the structural deformation in this polymer, the following coordinate may be chosen, as proposed by Castiglioni et al. [42].

$$R = \frac{1}{\sqrt{7}}(r_1 + r_3 + r_4 + r_6 - r_2 - r_5 - r_7) \tag{4-2}$$

where $r_i$s are shown in Figure 4-2b. The total energy of this polymer has only one minimum at $R_0$ as shown in Figure 4-2b. If we use the bond lengths, $r_1 = r_3 = r_4 = r_6 = 1.388$ Å, $r_2 = r_5 = 1.382$ Å, and $r_7 = 1.492$ Å, of the central unit of neutral *p*-terphenyl obtained by an ab initio MO calculation at the Hartree–Fock level with the double-zeta quality 3-21G basis set [43], $R_0$ is calculated to be 0.490 Å. As shown in Figure 4-2b, an increase in $R$ means the structural deformation toward a quinoid structure from a benzenoid structure.

## 4.4 Geometric Changes Induced by Doping

The main process of doping is a charge-transfer reaction between an organic polymer and a dopant. When charges are removed from (or added to) a polymer chain upon chemical doping, geometric changes occur over several repeating units and the charge is localized over this region. Structure parameters such as bond lengths, bond angles, etc. are changed in this region. For example, the bond lengths [44] of neutral *p*-terphenyl, its radical anion, and its dianion calculated by the PM3 method are shown in Table 4-1. From this table, we can see readily that the bond lengths of the neutral and charged species are different from each other. The phenyl and phenylene rings in neutral *p*-terphenyl have benzenoid structures. In the radical anion and dianion, an increase in $R$ occurs as the result of shortening of the $r_{23}$, $r_{45}$, and $r_{67}$ bonds and lengthening of the $r_{12}$, $r_{34}$, and $r_{56}$ bonds; in other words, geometric changes from benzenoid to quinoid occur upon ionization. The geometric

**Table 4-1.** Bond lengths (in Å) calculated by the PM3 method for *p*-terphenyl, its radical anion, and its dianion.

| Species | Bond length[a] | | | | | | Coordinate[b] |
|---|---|---|---|---|---|---|---|
| | $r_{12}$ | $r_{23}$ | $r_{34}$ | $r_{45}$ | $r_{56}$ | $r_{67}$ | $R$ |
| Neutral | 1.391 | 1.390 | 1.397 | 1.469 | 1.397 | 1.389 | 0.507 |
| Radical anion | 1.397 | 1.385 | 1.417 | 1.426 | 1.423 | 1.366 | 0.580 |
| Dianion | 1.400 | 1.371 | 1.438 | 1.388 | 1.446 | 1.351 | 0.640 |

[a] Numbering of carbon atoms is shown below. Dihedral angles between neighboring benzene rings are 48°, 0°, and 0° for *p*-terphenyl, its radical anion, and its dianion, respectively. The data are taken from [44].

[b] The structural deformation coordinate defined in Eq. 4-2 is calculated by using the equation, $R = 1/\sqrt{7}(4r_{56} - 2r_{67} - r_{45})$.

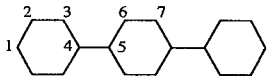


changes from the neutral species are larger for the dianion than for the radical anion. Since the localized charges, which are accompanied by geometric changes, can move along the polymer chain, they are regarded as charge carriers in conducting polymers. These quasiparticles are classified into polarons, bipolarons, and solitons according to their charge and spin.

### 4.4.1 Polarons, Bipolarons, and Solitons

Self-localized excitations and corresponding chemical terminologies are listed in Table 4-2. Schematic structures of the self-localized excitations in poly(*p*-phenylene) and *trans*-polyacetylene are depicted in Figure 4-3. In these illustrations, the charge and spin are localized on one carbon atom. In real polymers, however, they are considered to be localized over several repeating units with geometric changes.

When an electron is removed from an infinite polymer chain, charge $+e$ and spin 1/2 are localized over several repeating units with geometric changes. This is a self-localized excitation called a positive polaron (Figure 4-3a, e). Since a positive polaron has charge $+e$ and spin 1/2, it is a radical cation in chemical terminology. When an electron is added to a polymer chain, a negative polaron, which is a radical anion, is formed (Figure 4-3b, f).

When another electron is removed from a positive polaron, charge $+2e$ is localized over several repeating units. The charge $+2e$ is considered to be localized in a region narrower than that of a positive polaron. This species is called a positive bipolaron (Figure 4-3c). Since a positive bipolaron has charge $+2e$ and no spin, it is a dication in chemical terminology. A negative bipolaron corresponding to a dianion can also be considered (Figure 4-3d).

**Table 4-2.** Self-localized excitations and chemical terminologies.

| Self-localized excitation | Chemical term | Charge | Spin |
|---|---|---|---|
| positive polaron | radical cation | $+e$ | 1/2 |
| negative polaron | radical anion | $-e$ | 1/2 |
| positive bipolaron | dication | $+2e$ | 0 |
| negative bipolaron | dianion | $-2e$ | 0 |
| neutral soliton | neutral radical | 0 | 1/2 |
| positive soliton | cation | $+e$ | 0 |
| negative soliton | anion | $-e$ | 0 |

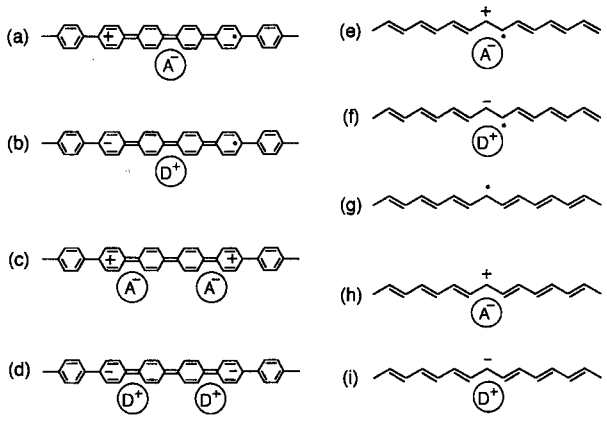


**Figure 4-3.** Schematic structures of self-localized excitations in poly(*p*-phenylene) and *trans*-polyacetylene. (a) Positive polaron; (b) negative polaron; (c) positive bipolaron; (d) negative bipolaron; (e) positive polaron; (f) negative polaron; (g) neutral soliton; (h) positive soliton; (i) negative soliton;. D, donor; A, acceptor; +, positive charge; −, negative charge; •, unpaired electron.

In *trans*-polyacetylene having a degenerate ground-state structure, soliton excitations can be formed between the A and B phases (see Figure 4-2a). Solitons are classified into neutral, positive, and negative types according to their charge. A neutral soliton has no charge and spin 1/2 (Figure 4-3g). A positive (or a negative) soliton has charge $+e$ (or $-e$) and no spin (Figure 4-3h, i). A neutral soliton, a positive soliton, and a negative soliton correspond, respectively, to a neutral radical, a cation, and an anion of a linear *trans*-oligoene with an odd number of carbon atoms, $C_nH_{n+2}$ (where $n$ is an odd number).

Bond-alternation defects or misfits in polyenes were studied using the Hückel MO method in the early 1960s [36, 45, 46], though these are nothing but solitons proposed by Su, Schrieffer, and Heeger [18, 19] about two decades after. These workers have studied solitons in *trans*-polyacetylene by using a simple tight-binding Hamil-

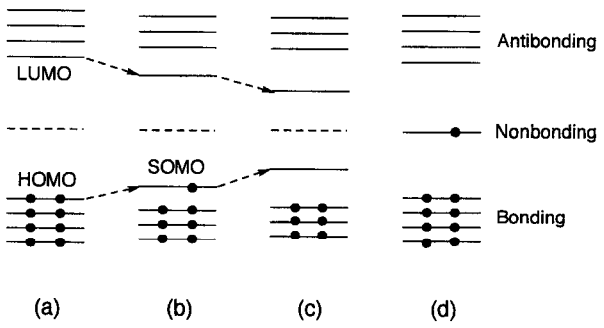


**Figure 4-4.** Schematic molecular orbital energy levels. (a) Neutral conjugated system; (b) its radical cation; (c) its dication; (d) neutral radical of an odd oligoene. HOMO, highest occupied molecular orbital; LUMO, lowest unoccupied molecular orbital; SOMO, singly occupied molecular orbital; •, electron.

tonian with an electron–lattice interaction term (SSH model), their model being essentially the same as the Hückel approximation. The continuum versions of the SSH model are very useful for describing polarons and bipolarons as well as solitons, because analytic solutions can be obtained for physical parameters (creation energy, electronic absorption, etc.) relating to the excitations [21, 47–49].

## 4.4.2 Electronic States of Polarons, Bipolarons, and Solitons

We will first discuss the electronic states of linear conjugated molecules at the Hückel level with electron–lattice interaction [7], as models of self-localized excitations. The MO energy levels of these systems are schematically shown in Figure 4-4. In a neutral conjugated molecule (e.g., *p*-terphenyl), the bonding and antibonding levels are formed as the result of interaction between π-electron levels (Figure 4-4a). In its radical cation, geometric changes lead to an upward shift of the highest occupied molecular orbital (HOMO) and a downward shift of the lowest unoccupied molecular orbital (LUMO), and one electron is removed from the HOMO level (Figure 4-4b); the singly occupied molecular orbital (SOMO) is then formed. In its radical anion, the HOMO level is occupied by two electrons and the LUMO has one electron. Since geometric changes in the dication, where another electron is removed from the HOMO level (Figure 4-4c), are larger than those in the radical cation, the HOMO and LUMO levels shift further. In the dianion, each of the HOMO and LUMO levels is occupied by two electrons. In the MO energy levels of an odd *trans*-oligoene radical, $C_nH_{n+2}^{\cdot}$ (where $n$ is an odd number), a nonbonding level, which is occupied by one electron, is formed in the center of the band gap as shown in Figure 4-4d [36]. In its cation and anion, the nonbonding level is occupied by null and two electrons, respectively.

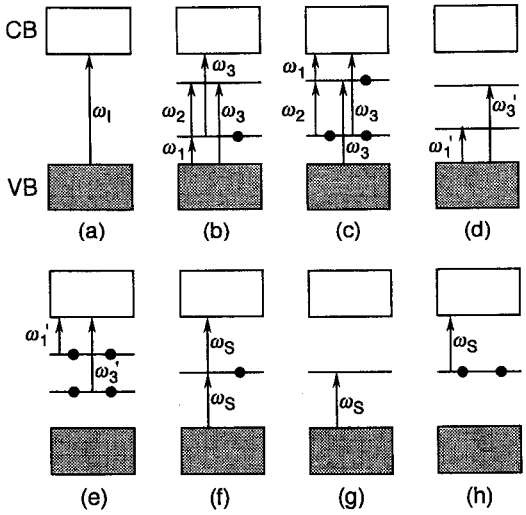


**Figure 4-5.** Schematic electronic band structures. (a) Neutral polymer; (b) positive polaron; (c) negative polaron; (d) positive bipolaron; (e) negative bipolaron; (f) neutral soliton; (g) positive soliton; (h) negative soliton. CB, conduction band; VB, valence band; •, electron; arrow, electronic transition.

Next, we discuss the electronic transitions due to polarons, bipolarons, and solitons in a polymer chain on the basis of a theoretical study reported by Fesser et al. [48] on a continuum electron–phonon-coupled model. The electronic energy levels of a neutral infinite polymer and those of polarons, bipolarons, and solitons are shown schematically in Figure 4-5.

In an infinite neutral polymer, interaction between repeating units leads to the formation of electronic energy bands. The bonding and antibonding levels constitute, respectively, the valence band (VB) and the conduction band (CB) as shown in Figure 4-5a. The band gaps ($\omega_I$ in Figure 4-5a) of most intact polymers are in the range between 35000 and 8000 $cm^{-1}$ (4.3 and 1.0 eV, 1 eV = 8066 $cm^{-1}$).

For a positive polaron (Figure 4-5b), two localized electronic levels, bonding and antibonding, are formed within the band gap. One electron is removed from the polaron bonding level. Thus, a positive polaron is expected to have the following three intragap transitions:

- $\omega_1$, polaron bonding level ← valence band
- $\omega_2$, polaron antibonding level ← polaron bonding level
- $\omega_3$, polaron antibonding level ← valence band, and conduction band ← polaron bonding level.

When a negative polaron is formed, one electron is added to the polaron antibonding level. In this case also, three transitions are expected (Figure 4-5c).

The electronic structure of a positive bipolaron is shown in Figure 4-5d. Since the geometric changes for a bipolaron are larger than those for a polaron, localized electronic levels appearing in the band gap for a bipolaron are farther away from the band edges than for a polaron. Two electrons are removed from the bipolaron

bonding level. Thus, a positive bipolaron is expected to have the following two intragap transitions:

- $\omega_1'$, bipolaron bonding level ← valence band
- $\omega_3'$, bipolaron antibonding level ← valence band.

When a negative bipolaron is formed, two electrons are added to the bipolaron antibonding level (Figure 4-5e) and thus two transitions are again expected. The intensities of the electronic transitions for polarons and bipolarons will be discussed in Section 4.7.1.2.

When a soliton is formed, a nonbonding electronic level is formed at the center of the band gap (Figure 4-5f–h). For a neutral soliton, the nonbonding electronic level is occupied by one electron, while for a positive soliton and a negative soliton, the level is occupied by null and two electrons, respectively. Thus, all the neutral, positive, and negative solitons are expected to have only one intragap transition, $\omega_s$, as shown in Figure 4-5f–h.

Polarons, bipolarons, and solitons are different from each other as described above. It is expected that we can detect these excitations separately by electronic absorption, ESR, and vibrational spectroscopies. In particular, geometric changes induced by doping can be studied by vibrational (Raman and infrared) spectroscopy.

## 4.5 Methodology of Raman Studies of Polarons, Bipolarons, and Solitons

Doping induces strong infrared absorptions that are attributed to the vibrational modes arising from charged domains generated by doping [10, 14, 15, 50]. In the case of *trans*-polyacetylene, Horovitz et al. [51–53] have proposed the amplitude-mode model for explaining doping-induced infrared absorptions. According to their theory, the normal vibrations that induce oscillations in bond alternation are strongly observed in the infrared spectra of doped polyacetylene. Castiglioni et al. [54] have reformulated the amplitude-mode theory in terms of the GF matrix method [55] used in molecular spectroscopy. In their treatment, they have proposed an effective conjugation coordinate (expressed by Eq. 4-1) which reflects bond alternation. They have also explained the doping-induced infrared absorptions of other conducting polymers such as polypyrrole, polythiophene, poly(*p*-phenylenevinylene), etc., by using effective conjugation coordinates [50]. However, the types of self-localized excitations (polarons, bipolarons, and solitons) existing in these doped polymers have not been identified.

Raman spectroscopy of conducting polymers has mainly treated the structures of intact polymers (geometry of polymer chains, conjugation length, force field, etc.) [13–15]. Although the Raman spectra of doped polymers have been reported [13–15], the observed Raman bands have not been correlated to the types of self-

localized excitations created by doping. Zerbi et al. [15] have drawn a conclusion from the effective-conjugation-coordinate model that the Raman bands arising from the charged domains are extremely weak and would never be observed. However, a new approach to Raman identification of the self-localized excitations will be described in this review.

Most of intact polymers show electronic absorptions in the region from ultraviolet to visible. Upon doping, new absorptions with several peaks appear in the region from visible to infrared. These new absorptions are associated with self-localized excitations created by doping. Thus, we can observe vibrational spectra arising from the charged domains, by using resonance Raman spectroscopy with a wide range of excitation wavelengths from visible to infrared [56, 57]. So far, although most of the Raman spectra of doped polymers have been measured by using visible laser lines for excitation, it is also desirable to use laser lines with longer wavelengths.

A useful method for analyzing the vibrational and electronic spectra of polymers is to compare them with the spectra of oligomers. In chemical terminology, polarons, bipolarons, and charged solitons are nothing but radical ions, divalent ions, and ions of oligomers, respectively (see Section 4.4.1). If these charged oligomers have geometries similar to those of self-localized excitations, these compounds would give rise to the electronic and Raman spectra similar to those of the self-localized excitations. We can identify self-localized excitations on the basis of the spectroscopic data for charged oligomers (charged oligomer approach) [56, 57].

## 4.6 Near-Infrared (NIR) Raman Spectrometry

Since the 1970s, Raman spectrometry has been using visible laser lines as the most common excitation sources. It was generally believed that NIR laser lines were not suitable for obtaining high-quality Raman spectra, though since Hirshfeld and Chase [58] and Fujiwara et al. [59] reported successful NIR Raman spectrometry measurements in 1986, this technique has advanced dramatically and NIR Raman spectrophotometers are now commercially available.

We will describe two NIR Raman spectrophotometers, one with a diffraction grating, and the other with an interferometer. A Ti: sapphire laser (Coherent Radiation 890) pumped with an argon ion laser (Coherent Radiation Innova 90-6) is used as an NIR source for Raman excitation. This laser covers the wavelength range between 680 and 1000 nm. Since the output intensity of the Ti: sapphire laser is very stable for a long time in comparison with a NIR dye laser, it is a good excitation source for NIR Raman spectrometry. Continuous-wave lasers are used for measuring the Raman spectra of doped polymers, because the doped samples are liable to damage due to high peak powers of pulsed lasers. Raman spectra are usually measured on a single polychromator (Spex 1870) equipped with a charge-coupled-device (CCD) detector (Princeton Instruments LN/CCD-1024TKBS, back-illuminated type, 1024 × 1024 pixels) operated at −120 °C. The CCD detector functions

with an ST-135 controller (Princeton Instruments) linked with an NEC PC-9801FX computer through an IEEE-488 interface. The spectroscopic response of the CCD detector extends to about 1000 nm. Optical filters (holographic notch filters) are used to eliminate the Rayleigh scattering. The advantage of this system lies in its high optical throughput due to the use of the single polychromator and optical filter.

We have modified an NIR Fourier-transform spectrophotometer (JEOL JIR-5500) for the measurements of Raman spectra excited with the 1064-nm line of a continuous-wave Nd:YAG laser (CVI YAG-MAX C-92) [60]. Raman-scattered radiation is collected with a 90° off-axis parabolic mirror in a back-scattering geometry. Collected radiation is passed through two or three long-wavelength-pass filters to reduce the Rayleigh scattering.

## 4.7 Poly(*p*-phenylene)

As a typical example, we will first discuss the results of the electronic absorption and Raman spectra of Na-doped poly(*p*-phenylene). Poly(*p*-phenylene) consists of benzene rings linked at the para positions as shown in Figure 4-1c. Since poly(*p*-phenylene) has a nondegenerate structure, polarons and/or bipolarons are expected to be formed by chemical doping. As model compounds of poly(*p*-phenylene), *p*-oligophenyls (abbreviated as PP*n*, *n* being the number of phenylene and phenyl rings) such as biphenyl (PP2), *p*-terphenyl (PP3), *p*-quaterphenyl (PP4), *p*-quinquephenyl (PP5), and *p*-sexiphenyl (PP6) are used. It has been shown by X-ray diffraction studies that the two phenyl rings of PP2 [61, 62] in crystal at room temperature are coplanar, and PP3 [63] and PP4 [64] in similar conditions deviate slightly from coplanarity. However, these deviations are not significant in analyzing their vibrational spectra. Accordingly, the phenylene and phenyl rings of PP5 and PP6 in solids, and poly(*p*-phenylene) are assumed to be coplanar.

### 4.7.1 Electronic Absorption Spectra

#### 4.7.1.1 Intact and Doped Poly(*p*-phenylene)

The electronic absorption spectra of undoped and electrochemically $Bu_4N^+$(n-type)-doped poly(*p*-phenylene) films are shown in Figure 4-6a, b, respectively [65, 66]. The undoped poly(*p*-phenylene) film shows the electronic absorption band at 27400 $cm^{-1}$ (365 nm), which is associated with the interband transition from the valence band to the conduction band. The value of the band gap ($\omega_I$ in Figure 4-5a) is estimated to be 24200 $cm^{-1}$ from the onset of the electronic absorption [66]. The electronic transition energies of PP*n* [67, 68] are plotted in Figure 4-7. The transition energy decreases as the chain length becomes longer, an observation explained by the fact that increased conjugation occurs for longer chains. The observed tran-

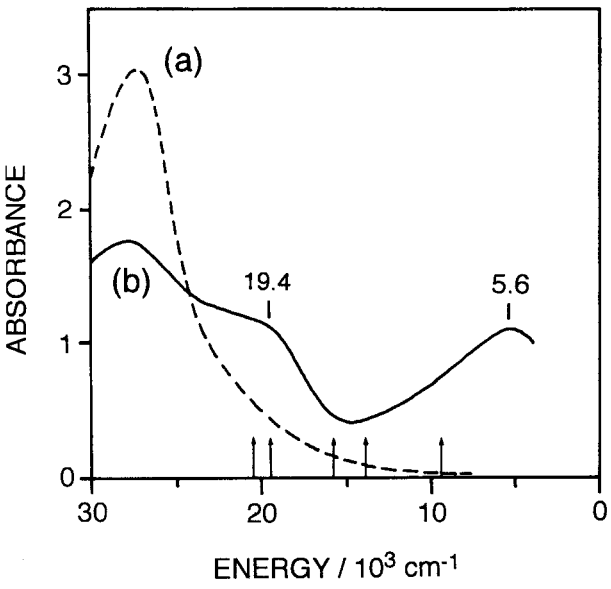


**Figure 4-6.** Absorption spectra of (a) undoped and (b) electrochemically $Bu_4N^+$(n-type)-doped poly(*p*-phenylene) films. Arrows indicate the positions of excitation wavelengths (488.0, 514.5, 632.8, 720, and 1064 nm) used for Raman measurements [66].

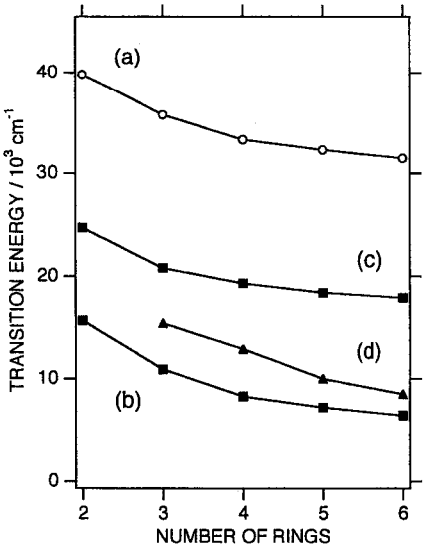


**Figure 4-7.** Observed electronic transition energies of *p*-oligophenyls. (a) Neutral species; (b) band I of the radical anions; (c) band II of the radical anions; (d) band I′ of the dianions. The data of neutral *p*-oligophenyls are taken from [67]. The data of the radical anions and dianions are taken from [69, 70].

sition energy of poly(*p*-phenylene), 27400 $cm^{-1}$, is lower than that of PP6, 31500 $cm^{-1}$, indicating that the conjugation length of poly(*p*-phenylene) is much longer than 6. Upon $Bu_4N^+$ doping, two broad absorptions appear at about 5600 $cm^{-1}$ (1800 nm) and 19400 $cm^{-1}$ (515 nm). The assignments of these bands will be discussed in the next section on the basis of the spectra of the radical anions ($PPn^{\cdot -}$)

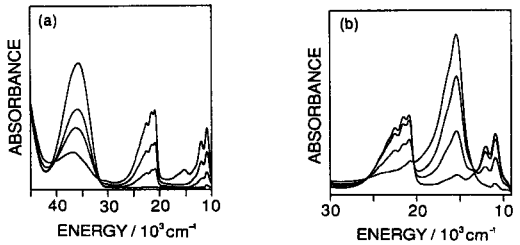


**Figure 4-8.** Absorption spectra of a THF solution of *p*-terphenyl at (a) early and (b) later stages of reduction. In (a), the 35600 $cm^{-1}$ band decreases and the 20800 and 10900 $cm^{-1}$ bands increase in intensity. In (b), the 20800 and 10900 $cm^{-1}$ bands decrease and the 15400 $cm^{-1}$ band increases in intensity.

and dianions ($PPn^{2-}$) of *p*-oligophenyls, which are models of negative polarons and bipolarons, respectively.

### 4.7.1.2 Radical Anions and Dianions of *p*-Oligophenyls

The electronic absorption spectra of $PPn^{\cdot-}$ and $PPn^{2-}$ have been systematically studied [69, 70]. When a tetrahydrofuran (THF) solution of PP3 is exposed to a sodium mirror, its absorption spectrum gives new bands (Figure 4-8). At an early stage, the band observed at 35700 $cm^{-1}$ (280 nm) arising from neutral PP3 decreases and the bands observed at 20800 and 10900 $cm^{-1}$ (481 and 916 nm) increase in intensity. These new bands are attributed to the radical anion of PP3 ($PP3^{\cdot-}$). In the course of this spectral change, an isosbestic point is observed at about 31500 $cm^{-1}$, indicating that PP3 is quantitatively converted into $PP3^{\cdot-}$. When the solution is further exposed to the sodium mirror, the 20800 and 10900 $cm^{-1}$ bands decrease and the band observed at 15400 $cm^{-1}$ (650 nm) increases in intensity. The 15400 $cm^{-1}$ band is ascribed to the dianion of PP3 ($PP3^{2-}$). During this reaction, three isosbestic points are observed at about 25800, 20400, and 13400 $cm^{-1}$. The THF solutions of PP*n* ($n = 4, 5$, and 6) show similar reduction reactions which may be described as

$$PPn + Na \rightarrow PPn^{\cdot-} + Na^{+}$$

$$PPn^{\cdot-} + Na \rightarrow PPn^{2-} + Na^{+}$$

Since $PPn^{\cdot-}$ is stable for a long time, we can conclude that the following disproportionation reaction does not occur.

$$2PPn^{\cdot-} \rightarrow PPn + PPn^{2-}$$

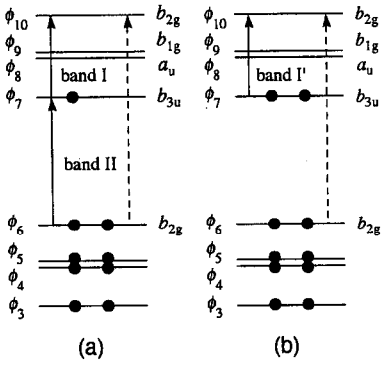


**Figure 4-9.** Schematic energy level diagrams. (a) The radical anion of biphenyl ($PP2^{\cdot -}$); (b) the dianion of biphenyl ($PP2^{2-}$). •, electron; arrow, electronic transition. The molecular orbital levels are taken from [77].

This reaction is similar to the process of the intramolecular formation of a bipolaron from two polarons.

The electronic transition energies [69, 70] of the radical anions and dianions of *p*-oligophenyls are plotted in Figure 4-7. Two strong bands are observed for the radical anions and are called bands I and II (curves b and c in Figure 4-7, respectively). On the other hand, one intense band is observed for the dianions, which is called band I′ (curve d in Figure 4-7). In the electronic absorption spectra of the radical cations and dications of α-oligothiophenes [71–73], two strong bands and one strong band are commonly observed for the radical cations and dications, respectively. In the case of the radical cations of oligophenylenevinylenes, two bands are observed [74, 75], although different results are also reported [76].

The absorption spectra of conducting polymers including poly(*p*-phenylene) have been discussed within the frame work of the Hückel approximation [7, 10]. In order to correlate the spectra of the radical anions and dianions of *p*-oligophenyls with those of doped poly(*p*-phenylene), we will discuss the observed absorption spectra of the charged *p*-oligophenyls on a similar theoretical basis. The energy diagram of $PP2^{\cdot -}$ is shown schematically in Figure 4-9a. Molecular orbital levels in this figure are taken from the results calculated by the Pariser–Parr–Pople–SCF–MO method for PP2 ($D_{2h}$ symmetry) [77]. A Pariser–Parr–Pople–SCF–MO–CI calculation for $PP2^{\cdot -}$ [78] shows that band I is assigned to the transition mostly attributable to the electronic excitation of $\phi_{10} \leftarrow \phi_7$ and band II to $\phi_7 \leftarrow \phi_6$. These transitions are polarized along the long molecular axis. The $\phi_8$ and $\phi_9$ levels are nonbonding with respect to the inter-ring CC bond. It is reasonable to consider that these assignments hold also for $PPn^{\cdot -}$ ($n = 3$–6). Moreover, band I′ of $PP2^{2-}$ is assigned to the transition mostly attributable to the electronic excitation $\phi_{10} \leftarrow \phi_7$ (Figure 4-9b). This assignment would also be applicable to $PPn^{2-}$ ($n = 3$–6). The $\phi_{10} \leftarrow \phi_6$ transitions of $PP2^{\cdot -}$ and $PP2^{2-}$ are symmetry forbidden under $D_{2h}$ symmetry.

Since the radical anions and dianions of *p*-oligophenyls correspond, respectively, to negative polarons and bipolarons in the polymer, bands I and II of the radical anions are associated, respectively, with the $\omega_1$ and $\omega_2$ transitions of polarons (Figure 4-5c), and band I′ of the dianions with the $\omega_1'$ transition of bipolarons (Figure 4-5e). The $\phi_{10} \leftarrow \phi_6$ transitions correspond to the $\omega_3$ and $\omega_3'$ transitions. It

is worthwhile pointing out that the $\omega_3$ and $\omega_3'$ transitions are symmetry forbidden. According to a continuum electron–phonon-coupled model reported by Fesser et al. [48], the $\omega_1$ and $\omega_2$ transitions are dominant among the three expected for a polaron, and the $\omega_1'$ transition is more intense between the two expected for a bipolaron. Finally, it is expected that *a polaron has two intense intragap transitions and a bipolaron one intense transition* [79].

The absorption spectrum of $Bu_4N^+$-doped poly(*p*-phenylene) can now be explained as follows. Two broad bands centered at about 5600 and 19400 $cm^{-1}$ (Figure 4-6) are attributable to the $\omega_1$ and $\omega_2$ transitions of negative polarons, respectively. These assignments will be discussed again in Section 4.7.3 on the basis of the Raman results.

## 4.7.2 Raman Spectra

### 4.7.2.1 Intact Poly(*p*-phenylene) and *p*-Oligophenyls

The observed infrared and Raman spectra of intact poly(*p*-phenylene) [80–84] have been analyzed by normal coordinate calculations [43, 84–87]. The factor group of a coplanar polymer is isomorphous with the point group $D_{2h}$. When the *yz* plane is taken in the phenylene-ring plane (*z* axis along the polymer chain) and the *x* axis perpendicular to the phenylene-ring plane, the irreducible representation at the zone center ($k = 0$) is as follows:

$$\Gamma^{vib}{}_{in\text{-}plane} = 5a_g(R) + 4b_{1u}(IR) + 4b_{2u}(IR) + 5b_{3g}(R)$$

$$\Gamma^{vib}{}_{out\text{-}of\text{-}plane} = 2a_u + 1b_{1g}(R) + 3b_{2g}(R) + 2b_{3u}(IR)$$

where R and IR denote Raman- and infrared-active vibrations, respectively. The 1064-nm excited Raman spectrum and infrared absorption spectrum of intact poly(*p*-phenylene) prepared by dehalogenation polycondensation of *p*-dihalogenobenzene are shown in Figure 4-10a, b, respectively. The observed and calculated vibrational frequencies of poly(*p*-phenylene), $^{13}C$-substituted analog, and perdeuterated analog are listed in Table 4-3, except for CH (CD) stretches [$\nu_1(a_g)$, $\nu_9(b_{1u})$, $\nu_{16}(b_{2u})$, and $\nu_{20}(b_{3g})$]. Major Raman and infrared bands have been assigned.

In Figure 4-10b, the 809 $cm^{-1}$ infrared band is assigned to the CH out-of-plane bend of the phenylene rings, and the 765 and 694 $cm^{-1}$ bands are assigned to the CH out-of-plane bends of the terminal phenyl rings.

The Raman spectrum of poly(*p*-phenylene) has been compared with those of *p*-oligophenyls. The 1064-nm excited Raman spectra of *p*-oligophenyls in the solid state [88] are shown in Figure 4-11. The bands at 1605–1593, 1278–1275, 1221–1220, and 795–774 $cm^{-1}$ correspond to those at 1595, 1282, 1222, and 798 $cm^{-1}$ of intact poly(*p*-phenylene), respectively. These bands are assigned to the $a_g$ vibrations ($\nu_2$–$\nu_5$). The atomic displacements of these modes obtained by normal coordinate calculations based on the PM3 method [84] are depicted in Figure 4-12a–d. The 1595 $cm^{-1}$ mode (Figure 4-12a) is contributed mainly by the CC stretch of the phenylene ring. The 1282 $cm^{-1}$ mode (Figure 4-12b) is mainly contributed by the

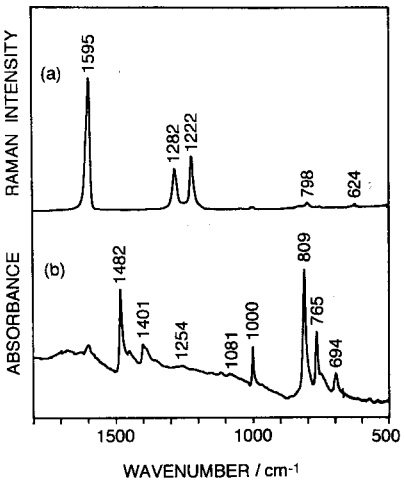


**Figure 4-10.** Vibrational spectra of intact poly(*p*-phenylene). (a) Raman spectrum taken with the 1064-nm line in powder sample; (b) infrared spectrum in a KBr disk [83].

inter-ring CC stretch. The 1222 $cm^{-1}$ mode (Figure 4-12c) is a mixture of CC stretch and CH in-plane bend. The 798 $cm^{-1}$ mode (Figure 4-12d) is a mixture of CC stretch and CCC deformation. The intensity of the 1278–1275 $cm^{-1}$ band relative to that of the 1221–1220 $cm^{-1}$ band decreases as the chain length becomes longer. Thus, this ratio is a marker of the length of conjugated segments [81, 82, 88]. The wavenumbers of the Raman bands of poly(*p*-phenylene) and *p*-oligophenyls are almost independent on the excitation wavelength [81]. It is well known that the wavenumbers of the two strong Raman bands of *trans*-polyacetylene depend greatly on the wavelength of the excitation laser. These large dispersions are explained by the existence of segments of various conjugation lengths that give rise to the Raman bands at different wavenumbers [13, 14]. However, the Raman spectra of other conducting polymers do not show such dependence on the excitation wavelength.

The (resonance) Raman intensities of conjugated molecules have been analyzed by the classical vibronic theory due to Tang and Albrecht [89]. Inagaki et al. [90] have shown that resonance Raman intensities of totally symmetric modes of $\beta$-carotene (an oligoene with eleven conjugated C=C bonds) arise from the A term (Franck–Condon term) of the Albrecht theory. Probably, the Franck–Condon factor plays an important role in determining the resonance Raman intensities of almost all conjugated molecules. The resonance Raman intensity of each totally symmetric mode is proportional to the square of the shift of the potential minimum in the resonant excited electronic state from that in the ground electronic state along the normal mode giving rise to the resonance Raman band, when the shift is small [91–94]. The effective conjugation coordinate represents approximately the change of equilibrium geometry between the ground electronic state and the first dipole-allowed excited electronic state [15]. Thus, the resonance Raman intensity of a normal mode is determined by the contribution of the effective conjugation coordinate to the mode. Details are described in [15]. It has been demonstrated that the

**Table 4-3.** Vibrational frequencies (in $cm^{-1}$) of neutral poly(*p*-phenylene) and its $^{13}C$-substituted and perdeuterated analogs.

| Symmetric species | No. | Normal species | | | | | $^{13}C$-substituted analog | | Perdeuterated analog | | |
|---|---|---|---|---|---|---|---|---|---|---|---|
| | | Observed | Calculated | | | | Observed | Calculated | Observed | Calculated | |
| | | [83] | [84] | [43] | [86] | [87] | [83] | [84] | [84] | [84] | [87] |
| $a_g$ | $\nu_2$ | 1595 | 1599 | 1626 | 1661 | 1601 | 1543 | 1547 | 1563 | 1563 | 1572 |
| | $\nu_3$ | 1282 | 1295 | 1282 | 1289 | 1290 | 1239 | 1246 | 1255 | 1281 | 1253 |
| | $\nu_4$ | 1222 | 1226 | 1233 | 1127 | 1184 | 1209 | 1216 | 892 | 887 | 863 |
| | $\nu_5$ | 798 | 776 | 792 | 846 | 802 | 768 | 747 | 764 | 751 | 776 |
| $a_u$ | $\nu_6$ | – | 969 | 951 | 961 | – | – | 960 | – | 775 | – |
| | $\nu_7$ | – | 427 | 367 | 401 | – | – | 415 | – | 378 | – |
| $b_{1g}$ | $\nu_8$ | – | 831 | 823 | 834 | – | – | 825 | – | 647 | – |
| $b_{1u}$ | $\nu_{10}$ | 1482 | 1477 | 1487 | 1510 | 1490 | 1452 | 1445 | 1354 | 1353 | 1364 |
| | $\nu_{11}$ | 1048 | 1060 | 1045 | 1051 | 1044 | – | 1035 | 817 | 812 | 811 |
| | $\nu_{12}$ | 1000 | 991 | 984 | 968 | 1004 | 965 | 958 | 978 | 984 | 977 |
| $b_{2g}$ | $\nu_{13}$ | – | 945 | 968 | 945 | – | – | 936 | – | 824 | – |
| | $\nu_{14}$ | – | 768 | 754 | 760 | – | – | 742 | – | 663 | – |
| | $\nu_{15}$ | – | 441 | 410 | 402 | – | – | 426 | – | 414 | – |
| $b_{2u}$ | $\nu_{17}$ | 1401 | 1407 | 1399 | 1440 | 1412 | 1361 | 1375 | 1338 | 1334 | 1347 |
| | $\nu_{18}$ | 1254 | 1232 | 1275 | 1268 | 1343 | – | 1193 | – | 1185 | 1268 |
| | $\nu_{19}$ | 1081 | 1119 | 1162 | 1075 | 1118 | – | 1092 | – | 854 | 855 |
| $b_{3g}$ | $\nu_{21}$ | – | 1603 | 1601 | 1654 | 1652 | – | 1546 | – | 1579 | 1620 |
| | $\nu_{22}$ | – | 1290 | 1325 | 1328 | 1343 | – | 1277 | – | 1016 | 1044 |
| | $\nu_{23}$ | 624 | 633 | 625 | 602 | 616 | 602 | 610 | 606 | 600 | 593 |
| | $\nu_{24}$ | – | 487 | 488 | 460 | 418 | – | 470 | – | 450 | 383 |
| $b_{3u}$ | $\nu_{25}$ | 809 | 798 | 797 | 790 | – | 801 | 789 | 650 | 661 | – |
| | $\nu_{26}$ | – | 497 | 457 | 458 | – | – | 481 | – | 435 | – |

Raman spectrum of neutral poly(*p*-phenylene) is well explained by the effective-conjugation-coordinate model [95].

### 4.7.2.2 Doped Poly(*p*-phenylene) and the Radical Anions and Dianions of *p*-Oligophenyls

The Raman spectra of heavily Na-doped poly(*p*-phenylene) measured with the 488.0, 514.5, 632.8, 720, and 1064 nm laser lines are shown in Figure 4-13 [70]. The Raman spectra of Na-doped poly(*p*-phenylene) are apparently different from that of intact poly(*p*-phenylene), indicating that these bands arise from charged domains (i.e., negative polarons and/or negative bipolarons) created by Na-doping. The assignments of these bands will be discussed on the basis of the data for the radical anions and dianions of *p*-oligophenyls.

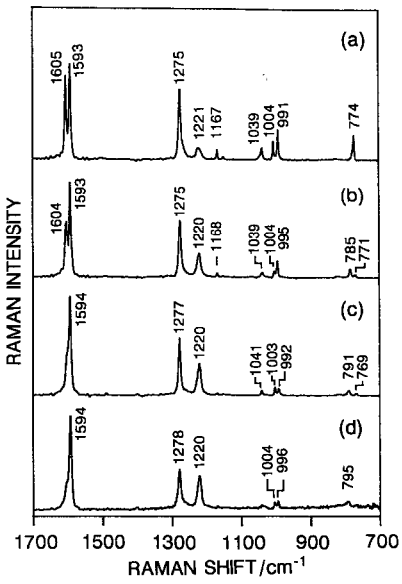


**Figure 4-11.** Raman spectra of *p*-oligophenyls in solid. (a) *p*-Terphenyl (PP3); (b) *p*-quaterphenyl (PP4); (c) *p*-quinquephenyl (PP5); (d) *p*-sexiphenyl (PP6). Excitation wavelength is 1064 nm [88].

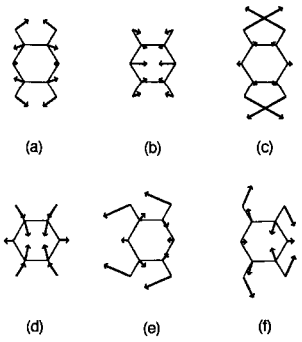


**Figure 4-12.** Atomic displacements of major vibrational modes ($k = 0$) of poly(*p*-phenylene). (a) 1599 $cm^{-1}$ [$\nu_2(a_g)$]; (b) 1295 $cm^{-1}$ [$\nu_3(a_g)$]; (c) 1226 $cm^{-1}$ [$\nu_4(a_g)$]; (d) 776 $cm^{-1}$ [$\nu_5(a_g)$]; (e) 1477 $cm^{-1}$ [$\nu_{10}(b_{1u})$]; (f) 991 $cm^{-1}$ [$\nu_{12}(b_{1u})$] [84].

The Raman spectra of the radical anions of PP2 [92, 96, 97], PP3 [70, 98], PP4 [70, 98], PP5 [70] and PP6 [70], and the dianions of PP3 [70, 98], PP4 [70, 98], PP5 [70], and PP6 [70] have been reported by several authors. The Raman spectra of the radical anions ($PPn^{\cdot -}$) and dianions ($PPn^{2-}$) in THF solutions are shown in Figures 4-14 and 4-15, respectively. The excitation wavelengths used are rigorously or nearly resonant with band II of the radical anions and band I′ of the dianions. The Raman spectra of the radical anions are similar to each other, and so are the Raman spectra of the dianions. However, the two groups of the Raman spectra are different from each other and from those of neutral *p*-oligophenyls. These results suggest that the negative polarons and bipolarons, corresponding respectively to the radical anions and dianions, can be identified by Raman spectroscopy.

The Raman spectra of the radical anions in Figure 4-14 show small changes with

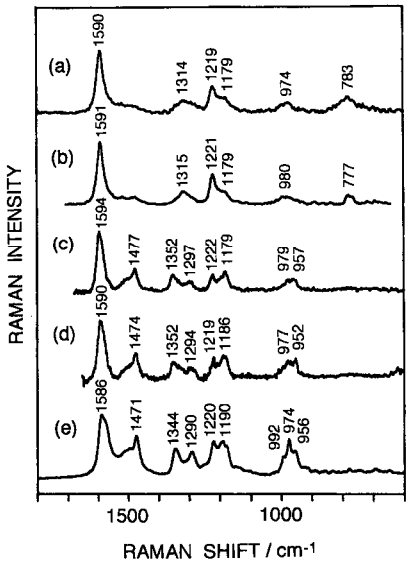


**Figure 4-13.** Raman spectra of Na-doped poly(-*p*-phenylene) taken with various wavelengths of excitation lasers. (a) 488.0; (b) 514.5; (c) 632.8; (d) 720, (e) 1064 nm [70].

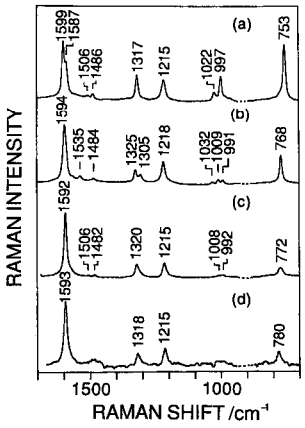


**Figure 4-14.** Resonance Raman spectra of the radical anions of *p*-oligophenyls in THF solutions. (a) *p*-Terphenyl; (b) *p*-quaterphenyl; (c) *p*-quinquephenyl; (d) *p*-sexiphenyl. Excitation wavelengths are 488.0 and 514.5 nm for (a) and (b–d), respectively. The bands of the solvent are subtracted [70].

the chain length. The intensities of the bands observed in the 1032–991 and 780–753 $cm^{-1}$ regions decrease as the chain length becomes longer, indicating that these bands are associated with the terminal rings. The bands observed in the 780–753 $cm^{-1}$ region show an upshift in wavenumber, as the chain length becomes longer. This result indicates that the wavenumbers of these bands can be used as a measure of the localization length of polarons. The bands observed in the 1325–1305 $cm^{-1}$ region are assigned to the inter-ring CC stretch [70, 92, 98]. The corresponding bands in neutral PP*n* are observed in the range between 1278 and 1275 $cm^{-1}$. About 40-$cm^{-1}$ upshifts are explained by the increased π-bond orders of the inter-ring CC bonds, i.e., shortening of the inter-ring CC bond lengths. In PP3, the calculated

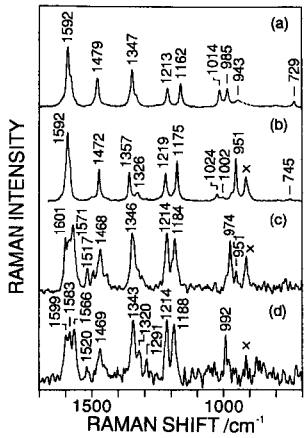


**Figure 4-15.** Resonance Raman spectra of the dianions of *p*-oligophenyls in THF solutions. (a) *p*-Terphenyl; (b) *p*-quaterphenyl; (c) *p*-quinquephenyl; (d) *p*-sexiphenyl. Excitation wavelengths are (a) 632.8, (b) 720, (c) 1064, and (d) 1064 nm, respectively. The bands with × are due to the solvent. Fluorescence background is subtracted in all the spectra [70].

length of the inter-ring CC bond ($r_{45}$) shrinks from 1.469 to 1.426 Å in going from neutral PP3 to $PP3^{\cdot -}$ (see Table 4-1).

In the Raman spectra of the dianions in Figure 4-15, the bands in the 1479–1468 $cm^{-1}$ and 1188–1162 $cm^{-1}$ regions are strongly observed. Corresponding bands are weakly observed or are not observed in the spectra of the radical anions. This reflects structural differences between the electronic ground state and the excited state associated with band II of the radical anions and band I′ of the dianions. The bands observed in the 1357–1320 $cm^{-1}$ region are assigned to the inter-ring CC stretch [70, 98]. About 70 $cm^{-1}$ upshifts in going from neutral PP*n* to $PPn^{2-}$ are also explained by the shortening of the inter-ring CC bond lengths. These upshifts of $PPn^{2-}$ are larger than those of $PPn^{\cdot -}$. This observation suggests that the degrees of shrinkage of the inter-ring CC bonds in $PPn^{2-}$ are larger than those in $PPn^{\cdot -}$. This is consistent with the results of calculation for PP3 given in Table 4-1: 1.469 Å (PP3) and 1.388 Å ($PP3^{2-}$). It is worth pointing out that the frequency of inter-ring CC stretch increases with the value of structural deformation coordinate *R* (column 8 in Table 4-1) for PP3, $PP3^{\cdot -}$, and $PP3^{2-}$. In the 1000–940 $cm^{-1}$ region, there is a series of bands at 943 ($PP3^{2-}$), 951 ($PP4^{2-}$), 974 ($PP5^{2-}$), and 992 $cm^{-1}$ ($PP6^{2-}$). This band series may be useful in estimating the localization length of bipolarons.

Next, we will analyze the Raman spectra of Na-doped poly(*p*-phenylene) (Figure 4-13) on the basis of those of the radical anions and dianions of *p*-oligophenyls. The Raman spectra of Na-doped poly(*p*-phenylene) taken with the 488.0- and 514.5-nm lines (Figure 4-13a, b) are different from those with the other three laser lines (Figure 4-13c–e), and are similar to those of the radical anions of *p*-oligophenyls (Figure 4-14). This observation can be understood by considering that the Raman bands arising from charged domains formed by Na-doping in the polymer chains are quite similar to those of the radical anions. Since the radical anions are viewed as negative polarons in the polymer, negative polarons exist in Na-doped poly(*p*-phenylene) [70]. These Raman spectra of Na-doped poly(*p*-phenylene) are observed under resonant conditions. Thus, the results described above indicate that the

**Table 4-4.** Observed Raman frequencies (in $cm^{-1}$) of negative polarons and negative bipolarons in Na-doped poly(*p*-phenylene).

| No. | Negative polaron[a] | Negative bipolaron[a] | Assignment[b] |
|---|---|---|---|
| A | 1591–1590 | 1594–1586 | sym. in-phase mode consisting of $\nu_2(a_g)$ |
| B | | 1477–1471 | sym., $\nu_{10}(b_{1u})$ |
| C | 1315–1314 | 1352–1344 | sym., in-phase, $\nu_3(a_g)$ |
| D | | 1297–1290 | sym., out-of-phase, $\nu_3(a_g)$ |
| E | 1221–1219 | 1222–1219 | sym., in-phase, $\nu_4(a_g)$ |
| F | 1179 | 1190–1179 | sym., out-of-phase, $\nu_4(a_g)$ |
| G | 980–974 | 992–952 | sym., $\nu_{12}(b_{1u})$ |
| H | 783–777 | | sym., in-phase, $\nu_5(a_g)$ |

[a] Data are taken from [83].

[b] Numbering and symmetry correspond to those of neutral poly(*p*-phenylene). Sym. denotes a symmetric mode.

absorption around 488.0 and 514.5 nm (20500 and 19400 $cm^{-1}$) is attributed to polarons.

The Raman spectra excited with laser lines in the 632.8–1064 nm region (Figure 4-13c–e) are quite similar to those of the dianions of *p*-oligophenyls (Figure 4-15), which correspond to negative bipolarons in the polymer. Accordingly, negative bipolarons also exist in Na-doped poly(*p*-phenylene), and the absorption in the 632.8–1064 nm (15800–9400 $cm^{-1}$) region arises from bipolarons [70]. In the 1000–950 $cm^{-1}$ region of the Raman spectra, a few bands are observed at 979 and 957 $cm^{-1}$ (632.8-nm excitation), at 977 and 952 $cm^{-1}$ (720 nm), and at 992, 974, and 956 $cm^{-1}$ (1064 nm). By comparing these bands with those of the Raman spectra of the dianions, it may be concluded that negative bipolarons localized over four, five, and six phenylene rings coexist in Na-doped poly(*p*-phenylene).

The Raman bands arising from negative polarons and bipolarons, together with the tentative mode assignments based on the wavenumber shifts upon $^{13}C$-substitution [83], are listed in Table 4-4. The observed bands are called bands A–H as shown in Table 4-4. Bands A, C, E, and H correspond to the $a_g$ modes ($\nu_i$, $i = 2$–5) of neutral poly(*p*-phenylene), respectively. The 1282 $cm^{-1}$ Raman band of neutral poly(*p*-phenylene) upshifts to 1315–1314 $cm^{-1}$ in the spectra of polarons and 1352–1344 $cm^{-1}$ in the spectra of bipolarons. According to normal coordinate calculations [43, 84, 86, 87], the 1282-$cm^{-1}$ mode is mainly attributed to the inter-ring CC stretch. The observed upshifts upon Na-doping reflect the increasing $\pi$-bond order of the inter-ring CC bond, i.e., structural changes from benzenoid to quinoid [70]. The upshifts for bipolarons (70–62 $cm^{-1}$) are larger than those for polarons (33–32 $cm^{-1}$), indicating that the geometric changes in bipolarons are larger than those in polarons. On the other hand, bands A and E show little shifts in wavenumber and band H shows a moderate shift.

In the Raman spectra of negative bipolarons (Figure 4-13c–e), bands B, D, F,

and G are strongly observed. Band B is assignable to a symmetric mode consisting of the $\nu_{10}(b_{1u})$ mode (Figure 4-12e) of each benzene ring in the charged domain. Band G is also attributed to a symmetric mode consisting of the $\nu_{12}(b_{1u})$ mode (Figure 4-12f). Bands D and F are assignable to out-of-phase symmetric modes consisting of the $\nu_3(a_g)$ and $\nu_4(a_g)$ modes (Figure 4-12b, c) of each benzene ring, respectively. The appearance of bands B, D, F, and G indicates the loss of translational symmetry of neutral poly(*p*-phenylene) chain, which is consistent with the formation of localized charged domains upon doping. Bands B, D, F, and G are not observed or weakly observed for negative polarons, but strongly observed for negative bipolarons. These observations seem to reflect different geometric changes occurring between polarons and bipolarons on going from their respective ground electronic states to their respective excited electronic states.

### 4.7.3 Assignments of Electronic Absorption Spectra of Doped Poly(*p*-phenylene)

In Section 4.7.1, two broad bands centered at about 5600 and 19400 $cm^{-1}$ in the electronic absorption spectrum of $Bu_4N^+$-doped poly(*p*-phenylene) have been attributed to the $\omega_1$ and $\omega_2$ transitions of negative polarons, respectively, on the basis of the data of the radical anions and dianions of *p*-oligophenyls. Raman spectroscopy provides information on the electronic levels associated with polarons and bipolarons as well as on their geometries. The Raman results indicate the coexistence of polarons and bipolarons in Na-doped poly(*p*-phenylene). The Raman bands due to polarons are resonantly enhanced by the use of the 488.0 and 514.5 nm laser lines, which are located within the electronic absorption around 19400 $cm^{-1}$ (515 nm). These observations confirm the proposed assignment that the 19400 $cm^{-1}$ band is due to the $\omega_2$ transition of polarons. The Raman bands due to bipolarons are resonantly enhanced by the use of the 632.8, 720, and 1064 nm laser lines. However, in the absorption spectrum of $Bu_4N^+$-doped poly(*p*-phenylene), no peaks are observed in the 15800–9400 $cm^{-1}$ (632.8–1064 nm) region. This fact can be explained by considering that the content of the bipolaron is very small and the $\omega_1'$ absorption due to the bipolaron is overlapped by the strong $\omega_1$ absorption band due to polarons.

## 4.8 Other Polymers

The Raman spectra of doped states of polyaniline [99], poly(*p*-phenylenevinylene) [75, 100–102], and polythiophene [72, 73] have been also analyzed on the basis of the data of charged oligomers (charged oligomer approach). The detected self-localized excitations are summarized in Table 4-5. Some important conclusions can be drawn from these Raman studies.

**Table 4-5.** Types of self-localized excitations detected by Raman spectroscopy.

| Polymer | Dopant | | | Species | Reference |
|---|---|---|---|---|---|
| | Type | Reagent | Content | | |
| poly(*p*-phenylene) | n | Na | heavy | polaron, bipolaron | [70] |
| poly(*p*-phenylenevinylene) | n | Na | heavy | polaron, bipolaron | [100] |
| | n | Na | light | polaron, bipolaron | [101] |
| | n | K | heavy | polaron, bipolaron | [101] |
| | p | $H_2SO_4$ | heavy | polaron | [75] |
| | p | $SO_3$ | heavy | polaron | [102] |
| | p | $SO_3$ | light | polaron | [102] |
| polythiophene | p | $BF_4^-$ | heavy | polaron | [72, 73] |
| polyaniline (emeraldine base form, 2A)[a] | p | HCl | heavy | polaron | [99] |
| polyaniline (leucoemeraldine, 1A) | p | $BF_4^-$ | heavy | polaron | [99] |

[a] HCl-doped emeraldine base form is called emeraldine acid form or 2S form.

1. Only polarons are detected for p-type doping. The Raman spectra of the polymers doped with acceptors do not show large changes with various excitation wavelengths [72, 73, 75]. The polymer-chain structures of p-type-doped polymers are more homogeneous, and more regular arrays of polarons are formed.
2. Polarons and bipolarons coexist in n-type doped polymers in contrast to the results of p-type doping. The Raman spectra of the polymers doped with donors depend on the excitation wavelength [70, 100]. These observations are explained by the existence of various localization lengths of polarons and/or bipolarons [70, 100]. The polymer-chain structures of the n-type-doped polymers are inhomogeneous. Possibly, Na-doped polymers are easily hydrogenated, even in the presence of a small amount of water during the sample preparation, and negative polarons and/or bipolarons are formed on the short conjugated segments.

The Raman spectra of doped polyacetylene have been reported with the excitation of visible laser lines [103–110]. There have been some discussions about the question of whether these bands arise from charged domains or undoped parts remaining in the doped films. Recently, the Raman spectra of maximally Na-doped polyacetylene excited with NIR lasers have been reported [57, 60, 111] and compared with those of the radical anions of $\alpha$, $\omega$-diphenyloligoenes and $\alpha$, $\omega$-dithienyloligoenes [111]. It has been concluded that the observed bands arise from charged domains (charged solitons and/or polarons), because the observed Raman spectra of the doped polymer are similar to those of the radical anions of $\alpha$, $\omega$-diphenyloligoenes. However, further studies are required for characterizing doped polyacetylene in more detail.

## 4.9 Electronic Absorption and ESR Spectroscopies and Theory

It is widely accepted [7, 10] that the major species generated by chemical doping in nondegenerate polymers is bipolarons, except for polyaniline. However, the results obtained from Raman spectroscopy indicate the existence of polarons at heavily doped polymers. These results are inconsistent with the established view. The experimental basis for claiming the existence of bipolarons has been electronic absorption and ESR spectra [7, 9, 10]. We will comment on these experimental results.

The electronic absorption spectra of p-type-doped polypyrrole have been interpreted in terms of polarons and bipolarons for the first time [112]. Electronic absorption spectra of doped polypyrrole in the range from visible to NIR show three bands due to intragap transitions at low dopant contents and two bands at high dopant contents [113]. The three bands are attributed to polarons and the two bands to bipolarons [112], because a polaron is expected to have three intragap transitions and a bipolaron is expected to have two intragap transitions (see Section 4.4.2). A quantitative ESR study [114] has confirmed the interpretation of the electronic absorption experiments. This rule of thumb for band assignment has so far also been applied to other conducting polymers.

However, the two electronic absorption bands of doped poly(*p*-phenylene) are not explained by bipolarons, as demonstrated in Section 4.7.3. Furthermore, p-type-doped polythiophene shows two absorptions at about 12000 and 5200 $cm^{-1}$ [72, 73, 115, 116] and p-type-doped poly(*p*-phenylenevinylene) shows two broad absorptions at about 19000 and 7300 $cm^{-1}$ [75, 117, 118]. In these two systems, only positive polarons are detected by Raman spectroscopy (see Table 4-5). These results of Raman spectroscopy suggest that the two-band pattern in the electronic absorption spectrum is attributed to polarons. As discussed in Section 4.7.1.2, it is expected that a polaron has two intense intragap transitions and a bipolaron one intense transition. From these findings, we propose a new rule: *a two-band pattern corresponds to polarons and one-band pattern to bipolarons* [79], when these species do not coexist. When polarons and bipolarons coexist, and their electronic absorptions are overlapped, a more careful examination of the observed spectrum is of course necessary.

Recently, Hill et al. [119] have proposed the existence of a singlet radical-cation dimer (i.e., polaron dimer) as an alternative to a spinless bipolaron to explain weak ESR signals from doped polymers. Their proposal is based on the observed dimerization of the radical cation of 2,5″-dimethylterthiophene. They have found by electronic absorption and ESR measurements that the above radical cation is dimerized at low temperature even at a low concentration ($4 \times 10^{-4}$ mol/l). Singlet intrachain polaron pairs and interchain polaron pairs give no ESR signals. Thus, the absence of ESR signals or observation of weak ESR signals does not directly lead to the conclusion that the doped polymer contains only bipolarons.

The stability of polarons, bipolarons, and solitons has been studied theoretically

under various models. According to the SSH model and similar approximations with electron–lattice coupling for a single polymer chain [7, 10], the creation energy of one bipolaron in a nondegenerate system (or two charged solitons in a degenerate system) is lower than that of two polarons. Thus, it is considered that two separate polarons are always unstable, and changed into a bipolaron (or two charged solitons). For doped polyacetylene, the effect of the electron–electron interaction and the dopant potential, which are not taken into account in the SSH model, have been studied [120]. On the other hand, the existence of polarons has been theoretically proposed by several authors. Kivelson and Heeger [121] have proposed a polaron lattice (regular infinite array of polarons) for explaining the metallic properties of heavily doped polyacetylene. Mizes and Conwell [122] have reported that polarons are stabilized in short conjugated segments for *trans*-polyacetylene and poly(*p*-phenylenevinylene) from the results obtained by a three-dimensional tight-binding calculation. Shimoi and Abe [123] have studied the stability of polarons and bipolarons in nondegenerate systems by using the Pariser–Parr–Pople method combined with the SSH model. A polaron lattice is stabilized by the electron–electron interaction at dopant contents lower than a critical concentration, whereas a bipolaron lattice is stabilized at dopant contents higher than the critical concentration. Thus, importance of the electron–electron interaction and three-dimensional interaction as well as the electron–lattice coupling has been demonstrated. However, the nature of the metallic states of heavily doped polymers remains an unresolved theoretical problem.

## 4.10 Mechanism of Charge Transport

Overall electrical conduction in doped polymers is considered to have contributions from various processes such as intrachain, interchain, interdomain, interfibril transport, etc. The contributions of individual processes would depend on the solid-state structure and morphology [8]. Charge transport has been discussed in terms of polarons, bipolarons, charged solitons, and their lattices [6, 8, 10]. Even when the dopant content is very small, electrical conductivity increases dramatically. At this doping level, discrete localized electronic levels associated with self-localized excitations are formed within the band gap, and the temperature dependencies of d.c. conductivity have been explained by the hopping between localized electronic states [8]. It is conceivable that the energy gap between the lower (or upper) localized state and the valence (or conduction) band for a positive (or a negative) polaron is smaller than that of a positive (or a negative) bipolaron. Then, it is expected that polarons play a more important role in hopping conduction than bipolarons.

Heavily doped polymers are of special interest, because these polymers show metallic properties such as a Pauli susceptibility, a linear temperature dependence of the thermoelectric power, a high reflectivity in the infrared region, etc., as described in Section 4.2. The temperature dependence of d.c. conductivity in heavily doped polymers is not like a metal, whereas metallic properties are observed. These results

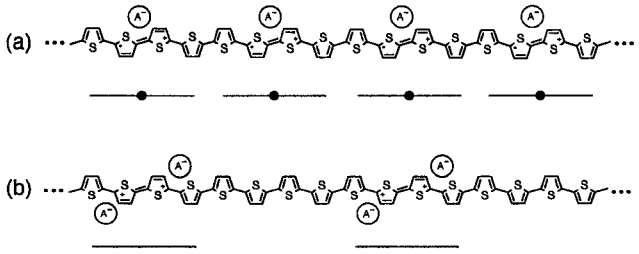


**Figure 4-16.** Schematic structures of polythiophene chains doped with electron acceptors (dopant content, 25 mole% per thiophene ring) and bonding electronic levels of positive polarons and bipolarons. (a) Polaron lattice; (b) bipolaron lattice. A, acceptor; +, positive charge; −, negative charge; •, electron; —, electronic energy level.

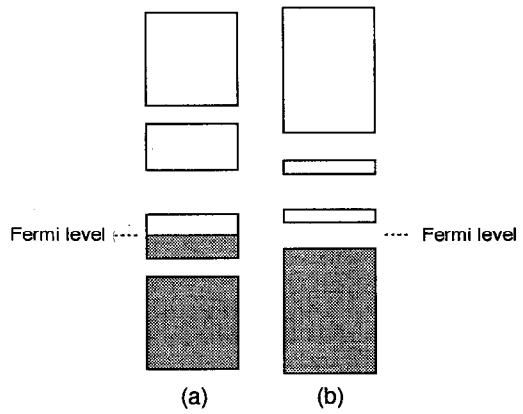


**Figure 4-17.** Schematic band structures of an infinite polymer chain doped with acceptors (dopant content, 25 mole% per thiophene ring). (a) Polaron lattice; (b) bipolaron lattice. Shadowed areas are filled with electrons [126].

can be explained as follows. Although a single chain itself behaves like a metal, macroscopic electrical conduction is limited by interchain, interdomain, or interfibril charge transport. Here, we will discuss the intrachain metallic charge transport.

Let us suppose an infinite nondegenerate polymer chain (e.g., polythiophene) doped heavily with electron acceptors. At a high dopant content, the polymer-chain structure and electronic structure of the doped polymer are radically different from those of the intact polymer. As typical cases, we will describe two kinds of lattice structures of doped polythiophene (dopant content, 25 mole% per thiophene ring): a polaron lattice and a bipolaron lattice. They are the regular infinite arrays of polarons and bipolarons. The schematic polymer-chain structures are shown in Figure 4-16. Band-structure calculations have been performed for polaron and/or bipolaron lattices of poly(*p*-phenylene) [124], polypyrrole [124], polyaniline [125], polythiophene [124, 126], and poly(*p*-phenylenevinylene) [127], with the valence-effective Hamiltonian pseudopotential method on the basis of geometries obtained by MO methods. The schematic electronic band structures shown in Figure 4-17

are based on the results calculated with this method for a polaron and a bipolaron lattice of p-type-doped polythiophene (dopant content, 25 mole% per thiophene ring) [126].

A polaron has a localized electronic level occupied by one electron (i.e., SOMO). In a polaron lattice formed at a heavy doping level, electronic wave functions of neighboring polarons are overlapped and interact with each other. As a result, a half-filled metallic band is formed from the polaron bonding levels occupied by one electron (Figure 4-17a). The Fermi level is located at the center of the polaron bonding band. The electronic states of the polaron lattice are not localized, whereas the electronic states of a polaron are localized. The calculated bandwidths of the polaron bands are 8900, 7900, and 5600 $cm^{-1}$ (1.1, 0.98, and 0.69 eV) for heavily doped polyaniline [125], polythiophene [126], and poly(*p*-phenylenevinylene) [127], respectively. If the conjugation length of the polymer chain is not sufficiently long, the metallic band is not formed. In this case, discrete levels are formed and hopping conduction is expected to take place. In contrast to the polaron lattice, no metallic band is formed for the bipolaron lattice, even if the conjugation length is long enough (Figure 4-17b). This is because a bipolaron has no singly occupied electronic level, whereas a polaron has a singly occupied level. In addition, the differences in the electronic band structure between the polaron and bipolaron lattices suggest that the bipolaron lattice is the result of a dimerization of the polaron lattice like the Peierls transition [126].

In the case of *trans*-polyacetylene (a degenerate polymer), band-structure calculations [126] indicate that a polaron lattice has a metallic band whereas a charged soliton lattice has no metallic band. An alternating polaron-charged soliton lattice [128] has been proposed for explaining the metallic properties of heavily doped states.

We will discuss polymer-chain structures obtained by Raman spectroscopy and metallic properties. The Raman measurements indicate the existence of positive polarons for p-type-doped polythiophene, poly(*p*-phenylenevinylene), and polyaniline at heavy doping levels (Table 4-5). These results indicate that positive polarons are formed on the polymer chains upon acceptor doping. If conjugation length is sufficiently long and the dopant content sufficiently high, a large number of polarons are formed and interact with each other. Then, a polaron lattice is formed. Therefore, the results of p-type-doped polythiophene, poly(*p*-phenylenevinylene), and polyaniline are consistent with the formation of polaron lattices at heavy doping levels. *The metallic properties observed for doped polymers probably originate from the polaron lattice.* From the results obtained so far, we can point out some important conditions for obtaining metallic polymers: (i) a long conjugation length; (ii) a high dopant content (large degree of charge transfer); and (iii) formation of polarons. In the case of n-type doping, both negative polarons and bipolarons are detected for doped poly(*p*-phenylene) and poly(*p*-phenylenevinylene) (Table 4-5). Polarons and bipolarons with various localization widths are detected, and electronic states are probably localized, even at heavy doping levels. It is considered that such an inhomogeneous structure does not lead to formation of a metallic band.

It is well known that physical properties of conducting polymers depend on

synthetic conditions, doping conditions, and other treatments of samples. Thus, in order to confirm the proposal that the metallic properties originate from the polaron lattice, it is requisite to use the same polymer film or the films from the same batch for measuring various physical properties and Raman spectra.

## 4.11 Summary

It has been demonstrated that Raman spectroscopy is a powerful tool for studying self-localized excitations such as polarons and bipolarons in doped conducting polymers. Resonance Raman spectroscopy by using exciting laser lines in a wide range between visible and near-infrared gives valuable information on self-localized excitations; especially, near-infrared Raman spectroscopy developed recently is important. Spectroscopic data on the radical ions and divalent ions of oligomers are useful for analyzing the electronic and vibrational spectra of doped polymers. New assignments of the electronic absorption spectra of polarons and bipolarons are proposed: a two-band pattern is attributed to polarons, and a one-band pattern to bipolarons. Polarons and/or bipolarons have been detected for doped poly(*p*-phenylene), polythiophene, poly(*p*-phenylenevinylene), and polyaniline by Raman spectroscopy. On the basis of the Raman results, metallic properties at heavily doped polymers is attributed to formation of a polaron lattice with a half-filled metallic band.

Postscript: After the manuscript of this Chapter was completed, a review book treating the polaron/bipolaron in conjugated polymers was published [129].

## 4.12 References

[1] Shirakawa, H., Louis, E. J., MacDiarmid, A. G., Chiang, C. K., Heeger, A. J., *J. Chem. Soc., Chem. Commun.* **1977**, 578–580.
[2] Chiang, C. K., Fincher, Jr., C. R., Park, Y. W., Heeger, A. J., Shirakawa, H., Louis, E. J., Gau, S. C., MacDiarmid, A.G., *Phys. Rev. Lett.* **1977**, *39*, 1098–1101.
[3] Wegner, G., *Angew. Chem. Int. Ed. Engl.* **1981**, *20*, 361–381.
[4] Etemad, S., Heeger, A. J., MacDiarmid, A. G., *Ann. Rev. Phys. Chem.* **1982**, *33*, 443–469.
[5] Baughman, R. H., Brédas, J. L., Chance, R. R., Elsenbaumer, R. L., Shacklette, L. W., *Chem. Rev.* **1982**, *82*, 209–222.
[6] Chien, J. C. W., *Polyacetylene–Chemistry, Physics, and Material Science*. New York: Academic Press, 1984.
[7] Brédas, J. L., Street, G. B. *Acc. Chem. Res.* **1985**, *18*, 309–315.
[8] Roth, S., Bleier, H., *Adv. Phys.* **1987**, *36*, 385–462.
[9] Patil, A. O., Heeger, A. J., Wudl, F., *Chem. Rev.* **1988**, *88*, 183–200.
[10] Heeger, A. J., Kivelson, S., Schrieffer, J. R., Su, W.-P., *Rev. Mod. Phys.* **1988**, *60*, 781–850.
[11] Kuzmany, H., Mehring, M., Roth, S. (Eds.) *Springer Ser. Solid-State Sci.* **1987**, 76; **1990**, 91 ; **1992**, 107.
[12] Lu, Y., *Solitons and Polarons*. Singapore: World Scientific, 1988.

[13] Kuzmany, H., *Makromol. Chem., Macromol. Symp.* **1990**, *37*, 81–97.
[14] Harada, I., Furukawa, Y., in: *Vibrational Spectra and Structure*: Durig, J. R. (Ed.). Amsterdam: Elsevier, 1991; Vol. 19, pp. 369–469.
[15] Gussoni, M., Castiglioni, C., Zerbi, G., in: *Advances in Spectroscopy*: Clark, R. J. H., Hester, R. E. (Eds.). Chichester: John Wiley & Sons, 1991; Vol. 19, pp. 251–353.
[16] Brédas, J. L., Silbey, R. (Eds.), *Conjugated Polymers*. Netherlands: Kluwer Academic Publishers, 1991.
[17] Tsukamoto, J., *Adv. Phys.* **1992**, *41*, 509–546.
[18] Su, W. P., Schrieffer, J. R., Heeger, A. J., *Phys. Rev. Lett.* **1979**, *42*, 1698–1701.
[19] Su, W. P., Schrieffer, J. R., Heeger, A. J., *Phys. Rev. B* **1980**, *22*, 2099–2111.
[20] Su, W. P., Schrieffer, J. R., *Proc. Natl. Acad. Sci. USA* **1980**, *77*, 5626–5629.
[21] Brazovskiĭ, S. A., Kirova, N. N., *Sov. Phys. JETP Lett.* **1981**, *33*, 4–8.
[22] Bishop, A. R., Campbell, D. K., Fesser, K., *Mol. Cryst. Liq. Cryst.* **1981**, *77*, 253–264.
[23] Brédas, J. L., Chance, R. R., Silbey, R., *Mol. Cryst. Liq. Cryst.* **1981**, *77*, 319–332.
[24] Ikehata, S., Kaufer, J., Woerner, T., Pron, A., Druy, M. A., Sivak, A., Heeger, A. J., MacDiarmid, A. G., *Phys. Rev. Lett.* **1980**, *45*, 1123–1126.
[25] Chung, T.-C., Moraes, F., Flood, J. D., Heeger, A. J., *Phys. Rev. B* **1984**, *29*, 2341–2343.
[26] Park, Y. W., Denenstein, A., Chiang, C. K., Heeger, A. J., MacDiarmid, A. G., *Solid State Commun.* **1979**, *29*, 747–751.
[27] Tanaka, M., Watanabe, A., Tanaka, J., *Bull. Chem. Soc. Jpn.* **1980**, *53*, 3430–3435.
[28] Kume, K., Mizuno, K., Mizoguchi, K., Nomura, K., Maniwa, Y., *Mol. Cryst. Liq. Cryst.* **1982**, *83*, 285–290.
[29] Moraes, F., Davidov, D., Kobayashi, M., Chung, T. C., Chen, J., Heeger, A. J., Wudl, F., *Synth. Met.* **1985**, *10*, 169–179.
[30] Kaneto, K., Hayashi, S., Ura, S., Yoshino, K., *J. Phys. Soc. Jpn.* **1985**, *54*, 1146–1153.
[31] Mizoguchi, K., Misoo, K., Kume, K., Kaneto, K., Shiraishi, T., Yoshino, K., *Synth. Met.* **1987**, *18*, 195–198.
[32] Lögdlund, M., Lazzaroni, R., Stafström, S., Salaneck, W. R., Brédas, J. L., *Phys. Rev. Lett.* **1989**, *17*, 1841–1844.
[33] Masubuchi, S., Kazama, S., *Synth. Met.*, **1995**, *74*, 151–158.
[34] Ginder, J. M., Richter, A. F., MacDiarmid, A. G., Epstein, A. J., *Solid State Commun.* **1987**, *63*, 97–101.
[35] Mizoguchi, K., Obana, T., Ueno, S., and Kume, K., *Synth. Met.* **1993**, *55*, 601–606.
[36] Salem, L., *The Molecular Orbital Theory of Conjugated Systems*. New York: Benjamin, 1966.
[37] Kohler, B. E., in: *Conjugated Polymers*: Brédas, J. L. and Silbey, R. (Eds.). Dordrecht: Kluwer Academic Publishers, 1991; pp. 405–434.
[38] Fincher, Jr., C. R., Chen, C.-E., Heeger, A. J., MacDiarmid, A. G., Hasting, J. B., *Phys. Rev. Lett.* **1982**, *48*, 100–104.
[39] Yannoni, C. S., Clarke, T. C., *Phys. Rev. Lett.* **1983**, *51*, 1191–1193.
[40] Villar, H. O., Dupuis, M., Watts, J. D., Hurst, G. J. B., Clementi, E., *J. Chem. Phys.* **1988**, *88*, 1003–1009.
[41] Hirata, S., Torii, H., Tasumi, M., *J. Chem. Phys.* **1995**, *103*, 8964–8979.
[42] Castiglioni, C., Gussoni, M., Zerbi, G., *Synth. Met.* **1989**, *29*, E1–E6.
[43] Cuff, L., Kertesz, M., *Macromolecules* **1994**, *27*, 762–770.
[44] Ohtsuka, H., Master's Thesis, The University of Tokyo, 1993.
[45] Longuet-Higgins, H. C., Salem, L., *Proc. Roy. Soc. A* **1959**, *251*, 172–185.
[46] Pople, J. A., Walmsley, S. H., *Mol. Phys.* **1962**, *5*, 15–20.
[47] Takayama, H., Lin-Liu, Y. R., Maki, K., *Phys. Rev. B* **1980**, *21*, 2388–2393.
[48] Fesser, K., Bishop, A. R., Campbell, D. K., *Phys. Rev. B* **1983**, *27*, 4804–4825.
[49] Onodera, Y., *Phys. Rev. B* **1984**, *30*, 775–785.
[50] Zerbi, G., Gussoni, M., Castiglioni, C., in: *Conjugated Polymers*: Brédas, J. L. and Silbey, R. (Eds.). Dordrecht: Kluwer Academic Publishers, 1991; pp. 435–507.
[51] Horovitz, B., *Solid State Commun.* **1982**, *41*, 729–734.
[52] Vardeny, Z., Ehrenfreund, E., Brafman, O., Horovitz, B., *Phys. Rev. Lett.* **1983**, *51*, 2326–2329.
[53] Ehrenfreund, E., Vardeny, Z., Brafman, O., Horovitz, B., *Phys. Rev. B* **1987**, *36*, 1535–1553.

[54] Castiglioni, C., Navarrete, J. T. L., Zerbi, G., Gussoni, M., *Solid State Commun.* **1988**, *65*, 625–630.
[55] Wilson, E. B., Decius, J. C., Cross, P. C., *Molecular Vibrations*. New York: MacGraw Hill, 1955.
[56] Furukawa, Y., *Springer Ser. Solid-State Sci.* **1992**, *107*, 137–143.
[57] Furukawa, Y., Sakamoto, A., Ohta, H., Tasumi, M., *Synth. Met.* **1992**, *49*, 335–340.
[58] Hirschfeld, T., Chase, B., *Appl. Spectrosc.* **1986**, *40*, 133–137.
[59] Fujiwara, M., Hamaguchi, H., Tasumi, M., *Appl. Spectrosc.* **1986**, *40*, 137–139.
[60] Furukawa, Y., Ohta, H., Sakamoto, A., Tasumi, M., *Spectrochim. Acta* **1991**, *47A*, 1367–1373.
[61] Trotter, J., *Acta Cryst.* **1961**, *14*, 1135–1140.
[62] Hargreaves, A., Rizvi, S. H., *Acta Cryst.* **1962**, *15*, 365–373.
[63] Baudour, J. L., Cailleau, H., Yelon, W. B., *Acta Cryst.* **1977**, *B33*, 1773–1780.
[64] Delugeard, Y., Desuche, J., Baudour, J. L., *Acta Cryst.* **1976**, *B32*, 702–705.
[65] Tabata, M., Satoh, M., Kaneto, K., Yoshino, K., *J. Phys. Soc. Jpn.* **1986**, *55*, 1305–1310.
[66] Satoh, M., Tabata, M., Uesugi, F., Kaneto, K., Yoshino, K., *Synth. Met.* **1987**, *17*, 595–600.
[67] Gillam, A. E., Hey, D. H., *J. Chem. Soc.* **1939**, 1170–1177.
[68] Dale, J., *Acta Chem. Scand.* **1957**, *11*, 650–659.
[69] Balk, P., Hoijtink, G. J., Schreurs, J. W. H., *Rec. Trav. Chim.* **1957**, *76*, 813–823.
[70] Furukawa. Y., Ohtsuka, H., Tasumi, M., *Synth. Met.* **1993**, *55*, 516–523.
[71] Fichou, D., Horowitz, G., Xu, B., Garnier, F., *Synth. Met.* **1990**, *39*, 243–259.
[72] Furukawa, Y., Yokonuma, N., Tasumi, M., Kuroda, M., Nakayama, J., *Mol. Cryst. Liq. Cryst.* **1994**, *256*, 113–120.
[73] Yokonuma, N., Furukawa, Y., Tasumi, M., Kuroda, M., Nakayama, J., *Chem. Phys. Lett. Chem. Phys. Lett.* **1996**, *255*, 431–436.
[74] Deussen, M., Bässler, H., *Chem. Phys.* **1992**, *164*, 247–257.
[75] Sakamoto, A., Furukawa, Y., Tasumi, M., *J. Phys. Chem.* **1994**, *98*, 4635–4640; *J. Phys. Chem.* **1997**, *101*, 1726–1732; Furukawa, Y., Sakamoto, A., Tasumi, M. *Macromol. Symp.* **1996**, *101*, 95–102.
[76] Spangler, C. W., Hall, T. J., *Synth. Met.* **1991**, *44*, 85–93.
[77] Dewar, M. J. S., Trinajstić, N., *Czech. Chem. Commun.* **1970**, *35*, 3136–3189.
[78] Zahradník, R., Cársky, P., *J. Phys. Chem.* **1970**, *74*, 1240–1248.
[79] Furukawa, Y., *Synth. Met.*, **1995**, *69*, 629–632; *J. Phys. Chem.* **1997**, *100*, 15644–15653.
[80] Shacklette, L. W., Chance, R. R., Ivory, D. M., Miller, G. G., Baughman, R. H., *Synth. Met.* **1979**, *1*, 307–320.
[81] Krichene, S., Lefrant, S., Froyer, G., Maurice, F., Pelous, Y., *J. Phys. Colloq.* **1983**, *44*, 733–736.
[82] Krichene, S., Buisson, J. P., Lefrant, S., *Synth. Met.* **1987**, *17*, 589–594.
[83] Furukawa, Y., Ohtsuka, H., Tasumi, M., Wataru, I., Kanbara, T, Yamamoto, T., *J. Raman Spectrosc.* **1993**, *24*, 551–554.
[84] Ohtsuka, H., Furukawa, Y., Tasumi, M., Wataru, I., Yamamoto, T., unpublished work.
[85] Rakovic, D., Bozovic, I., Stepanyan, S. A., Gribov, L. A., *Solid State Commun.* **1982**, *43*, 127–129.
[86] Zannoni, G., Zerbi, G., *J. Chem. Phys.* **1985**, *82*, 31–38.
[87] Buisson, J. P., Krichène, S., Lefrant, S., *Synth. Met.* **1987**, *21*, 229–234.
[88] Ohtsuka, H., Furukawa, Y., Tasumi, M., *Spectrochim. Acta* **1993**, *49A*, 731–737.
[89] Tang, J., Albrecht, A. C., in: *Raman Spectroscopy*: Szymanski, H. (Ed.). New York: Plenum, 1970; Vol. 2, pp. 33–68.
[90] Inagaki, F., Tasumi, M., Miyazawa, T., *J. Mol. Spectrosc.* **1974**, *50*, 286–303.
[91] Warshel, A., Dauber, P., *J. Chem. Phys.* **1977**, *66*, 5477–5488.
[92] Yamaguchi, S., Yoshimizu, N., Maeda, S., *J. Phys. Chem.* **1978**, *82*, 1078–1080.
[93] Peticolas, W. L., Blazej, D. C., *Chem. Phys. Lett.* **1979**, *63*, 604–608.
[94] Kakitani, H., *Chem. Phys. Lett.* **1979**, *64*, 344–347.
[95] Cuff, L., Kertestz, M., *J. Phys. Chem.* **1994**, *98*, 12223–12231.
[96] Takahashi, C., Maeda, S., *Chem. Phys. Lett.* **1974**, *24*, 584–588.
[97] Aleksandrov, I. V., Bobovich, Ya. S., Maslov, V. G., Sidorov, A. N., *Opt. Spectrosc.* **1975**, *38*, 387–389.

[98] Matsunuma, S., Yamaguchi, S., Hirose, C., Maeda, S., *J. Phys. Chem.* **1988**, *92*, 1777–1780.
[99] Furukawa, Y., Ueda, F., Hyodo, Y., Harada, I., Nakajima, T., Kawagoe, T., *Macromolecules* **1988**, *21*, 1297–1305.
[100] Sakamoto, A., Furukawa, Y., Tasumi, M., *J. Phys. Chem.* **1992**, *96*, 3870–3874.
[101] Sakamoto, A., Furukawa, Y., Tasumi, M., *Synth. Met.* **1993**, *55*, 593–598.
[102] Sakamoto, A., Furukawa, Y., Tasumi, M., Noguchi, T., Ohnishi, T., *Synth. Met.* **1995**, *69*, 439–440.
[103] Harada, I., Furukawa, Y., Tasumi, M., Shirakawa, H., Ikeda, S., *J. Chem. Phys.* **1980**, *73*, 4746–4757.
[104] Kuzmany, H., *Phys. Stat. Sol. B* **1980**, *97*, 521–531.
[105] Furukawa, Y., Harada, I., Tasumi, M., Shirakawa, H., Ikeda, S., *Chem. Lett.* **1981**, 1489–1492.
[106] Schügerl, B., Kuzmany, H., *Phys. Stat. Sol. B* **1982**, *111*, 607–617.
[107] Faulques, E., Lefrant, S., *J. Phys. Colloq.* **1983**, *44*, 337–340.
[108] Eckhardt, H., Shacklette, L. W., Szobota, J. S., Baughman, R. H., *Mol. Cryst. Liq. Cryst.* **1985**, *117*, 401–409.
[109] Tanaka, J., Saito, Y., Shimizu, M., Tanaka, C., Tanaka, M., *Bull. Chem. Soc. Jpn.* **1987**, *60*, 1595–1605.
[110] Mulazzi, E., Lefrant, S., *Synth. Met.* **1989**, *28*, D323–D329.
[111] Furukawa, Y., Uchida, Y., Tasumi, M., Spangler, C. W., *Mol. Cryst. Liq. Cryst.* **1994**, *256*, 721–726; Kim, J.-Y., Ando, S., Sakamoto, A., Furukawa, Y., Tasumi, M., *Synth. Met.* **1997**, *89*, 149–152.
[112] Brédas, J. L., Scott, J. C., Yakushi, K., Street, G. B., *Phys. Rev. B* **1984**, *30*, 1023–1025.
[113] Yakushi, K., Lauchlan, L. J., Clarke, T. C., Street, G. B., *J. Chem. Phys.* **1983**, *79*, 4774–4778.
[114] Nechtschein, M., Devreux, F., Genoud, F., Vieil, E., Pernaut, J. M., Genies, E., *Synth. Met.* **1986**, *15*, 59–78.
[115] Chung, T.-C., Kaufman, J. H., Heeger, A. J., and Wudl, F., *Phys. Rev. B* **1984**, *30*, 702–710.
[116] Kaneto, K., Kohno, Y., and Yoshino, K., *Mol. Cryst. Liq. Cryst.* **1985**, *118*, 217–220.
[117] Bradley, D. D. C., Evans, G. P., and Friend, R. H., *Synth. Met.* **1987**, *17*, 651–656.
[118] Voss, K. F., Foster, C. M., Smilowitz, L., Mihailović, D., Askari, S., Srdanov, G., Ni, Z., Shi, S., Heeger, A. J., and Wudl, F., *Phys. Rev. B* **1991**, *43*, 5109–5118.
[119] Hill, M. G., Mann, K. R., Miller, L. L., Penneau, J.-F., *J. Am. Chem. Soc.* **1992**, *114*, 2728–2730.
[120] Stafström, S., in: *Conjugated Polymers*: Brédas, J. L. and Silbey, R. (Eds.). Dordrecht: Kluwer Academic Publishers, 1991; pp. 113–140.
[121] Kivelson, S., Heeger, A. J., *Phys. Rev. Lett.* **1985**, *55*, 308–311.
[122] Mizes, H. A., Conwell, E. M., *Phys. Rev. Lett.* **1993**, *70*, 1505–1508.
[123] Shimoi, Y., Abe, S., *Phys. Rev. B* **1994**, *50*, 14781–14784.
[124] Brédas, J. L., Thémans, B., Fripiat, J. G., André, J. M., Chance, R. R., *Phys. Rev. B* **1984**, *29*, 6761–6773.
[125] Stafström, S., Brédas, J. L., Epstein, A. J., Woo, H. S., Tanner, D. B., Huang, W. S., MacDiarmid, A. G., *Phys. Rev. Lett.* **1987**, *59*, 1464–1467.
[126] Stafström, S., Brédas, J. L., *Phys. Rev. B* **1988**, *38*, 4180–4191.
[127] Brédas, J. L., Beljonne, D., Shuai, Z., Toussaint, J. M., *Synth. Met.* **1991**, *43*, 3743–3746.
[128] Tanaka, C., Tanaka, J., *Synth. Met.* **1993**, *57*, 4377–4384.
[129] Sariciftci, N. S. (Ed.) *Primary Photoexcitations in Conjugated Polymers: Molecular Exciton versus Semiconductor Band Model*. Singapore: World Scientific, 1997, Chapter 17.